Available online at www.sciencedirect.com
SCIENCE DIRECT®
Solar Energy Materials & Solar Cells
ELSEVIER
Solar Energy Materials & Solar Cells 83 (2004) 247–262
www.elsevier.com/locate/solmat

# Patterns of efficiency and degradation of composite polymer solar cells

T. Jeranko[a], H. Tributsch[a,*], N.S. Sariciftci[b], J.C. Hummelen[c]

[a] *Dept. Solare Energetik, Hahn-Meitner-Institut, Glienicker Str. 100, Berlin 14109, Germany*
[b] *Department of Physical Chemistry, Linz Institute for Organic Solar Cells (LIOS), Johann Kepler University of Linz, Altenbergerstr. 69, Linz A-4040, Austria*
[c] *Molecular Electronics, Materials Science Centre Plus, University of Groningen, Nijenborgh 4, Groningen 9747 AG, The Netherlands*

**Abstract**

Bulk-heterojunction plastic solar cells (PSC) produced from a conjugated polymer, poly(2-methoxy-5-(3′,7′-dimethyloctyl-oxy)-1,4-phenylenevinylene) (MDMO-PPV), and a methanofullerene [6,6]-phenyl $C_{61}$-butyric acid methyl ester (PCBM) were investigated using photocurrent imaging techniques to determine characteristic patterns of efficiency and degradation. The solar cells with power efficiencies of up to 2.6% showed significant inhomogeneities and variations depending on the preparation steps (e.g. aluminum deposition), suggesting there is still room for improvements. A characteristic feature of the well-known photoinduced and dark cell degradation is the formation of islands of higher efficiency. Degradation mechanisms appear to have a morphological component. The imaging technique will open opportunities for combinatorial plastic solar cell research.


*Keywords:* Plastic solar cells; Photocurrent; Imaging techniques; Degradation mechanisms

## 1. Introduction

Plastic solar cells consisting of thin films of solid-state composites of conjugated polymer/fullerene have attracted significant attention [1–6]. In contrast to traditional heterojunction photovoltaic cells, plastic solar cells are based on irreversible charge separation in the micro-heterogeneous bulk. This is achieved by

*Corresponding author. Tel.: +49-30-80622247; fax: +49-30-80622434.
*E-mail address:* tributsch@hmi.de (H. Tributsch).

0927-0248/$ - see front matter © 2004 Elsevier B.V. All rights reserved.
doi:10.1016/j.solmat.2004.02.028

homogenous distribution of the fullerene acceptor in the polymer donor matrix. Recently, plastic solar cells produced from a conjugated polymer poly(2-methoxy-5-(3′,7′-dimethyloctyl-oxy)-1,4-phenylenevinylene) (MDMO-PPV) and a methanofullerene [6,6]-phenyl $C_{61}$-butyric acid methyl ester (PCBM) have received much attention. Our contribution will focus on this type of composite polymer solar cell. The presently still high photoinstability and dark instability of plastic solar cells is a well-known challenge. It has motivated experimental strategies focused on glove boxes with controlled atmospheres. An important goal is to understand and tackle the mechanisms of instability, and to eventually avoid expensive manufacturing techniques. This contribution aims at investigating plastic solar cells by means of photocurrent imaging techniques in order to identify characteristic spatial patterns of efficiency and degradation.

## 2. Experimental

### 2.1. Summary of cell fabrication

The preparation steps used in cell preparation are explained in Fig. 1. ITO/glass substrates (MDT Darmstadt; Praezisions Glas und Optik) were structured with a laser and cleaned in ultrasonic baths. Buffer layers for acceptor strength modulation were deposited by spin-casting poly(3,4-ethylenedioxythiophene):polystyrene sulfonic acid (PEDOT: PSS, Bayer AG) in air. The active layer was cast from a chlorobenzene solution with mass ratios of MDMO-PPV and metanofullerene (PCBM) of (1:5). Deposition of the top electrode was done by thermal evaporation of Al through a shadow mask to define a device area of about 5 $mm^2$. All Al electrodes were non-transparent with a measured thickness of ca. 40 nm. Spin casting of active layers was performed under a dry argon atmosphere to avoid photooxidation of the fragile layers. After evaporation of the metal electrode, devices were characterized in a sealed container (see Fig. 2) under an argon atmosphere or in air.

#### 2.1.1. Preparation of samples

Squares of ITO-coated glass ($15 \times 15 \times 1\,mm^3$) were laser-structured (Fig. 1) to avoid short circuits in the finished cells. The samples were cleaned in acetone and isopropanol ultrasonic baths, consecutively, and blow-dried under pressurized argon. The cleaned substrates were stored in a glove box.

#### 2.1.2. Spin casting of the buffer layer

PEDOT: PPS, Bayer AG was filtered using a 0.4 μm membrane filter, mixed 1:1 with water and stirred for 2 h. The solution was spin cast onto the prepared ITO substrates in air in two steps using 1500 RPM for 20 s and 2000 RPM for 40 s. After each step, a slab of ITO was wiped clear of buffer with cotton wool and acetone. The

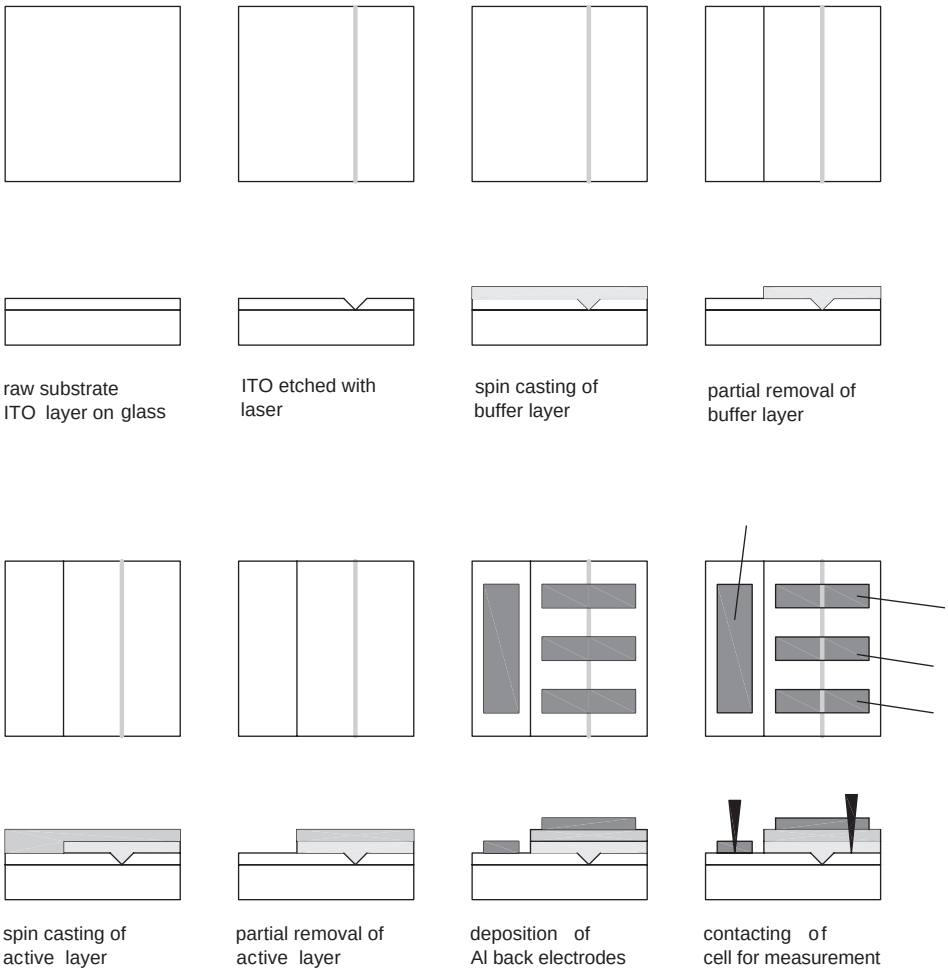


Fig. 1. Preparation steps for cell fabrication.

samples were then dried under a vacuum and transferred to a glove box for spin casting of the active layer.

*2.1.3. Spin casting of the active layer*

The complete process was performed under an inert argon atmosphere. PCBM was weighed and dissolved in chlorobenzene to give a 1% w/w solution. The solution was stirred for 24 h. MDMO-PPV was added (mass ratio PCBM:MDMO-PPV 5:1) and the solution stirred for another 2 h. It was then heated to 50°C for 10 min and spin cast onto the prepared samples in two steps using 1500 RPM for 20 s and 2000 RPM for 40 s. The solution was kept at constant

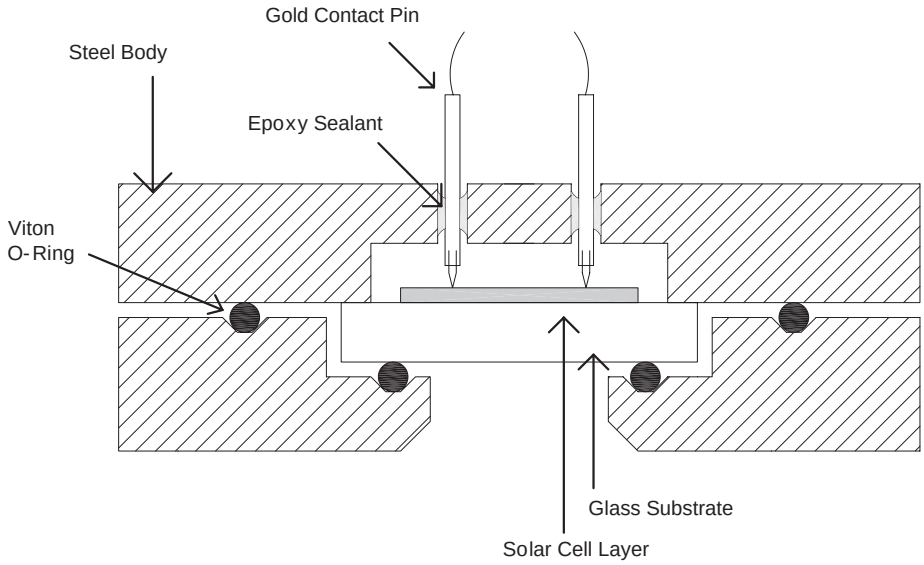


Fig. 2. Sealed box for solar cell characterization.

temperature and in the dark during the process. After each step, the same slab as in Section 2.1.2 (see Fig. 1) was wiped clear of coating with cotton wool and toluene.

### 2.1.4. Deposition of aluminum layer

Al layers were deposited by vaccum evaporation, aiming to achieve a 40 nm thickness. Samples were placed on masks defining selected areas of the cells. To avoid a gradient in layer thickness the samples were rotated during the deposition process. The vaccum chamber was evacuated with a turbomolecular pump. Typical pressures during deposition were $10^{-7}$ mbar. Aluminum was heated in a thin ceramic tube at the base of the chamber, ca. 50 cm below the samples, kept at a storage temperature of ca. 200°C. The Al was first slowly heated to about 1000°C and then to about 1300°C. When the deposition rate was measured to be 0.1 nm/s, a shutter was opened to allow deposition onto the samples, keeping the rate constant. Typically, it took 10–15 min to deposit 40 nm. No LiF was applied below the Al layer. After depositon, the chamber was flushed with argon and the samples stored in an inert adjacent chamber.

## 2.2. Scanning apparatus

The experimental technique used for most measurements presented in this contribution is the scanning microscope for semiconductor characterization (SMSC) [7,8]. The cells are mounted on a scan stage which allows the movement of the probe in the $x$ and $y$ directions. A He–Ne laser (632 nm) is focussed on the cell in a

small spot, and the resulting photocurrent is measured point by point. The current induced by the laser beam is filtered out from the background using a lock-in amplifier. The spatially resolved photocurrent images were obtained by scanning across the sample in this way. The image resolution depends on the size of the laser spot focused through the microscope lenses and the scan-step-width, though the former is the limiting factor. The spot diameter was varied between 10 and 30 μm except for the higher-resolution images (Fig. 10) when a 2 μm spot diameter was selected.

The experimental conditions applied in the scanning measurements and the measurement program selected for the different samples are shown in detail in Table 1.

### 2.3. Current–voltage curve measurement

Current–voltage curves were recorded under a calibrated solar simulator, adjusted to 1000 $W/m^2$. During the measurements, cells were inside a portable airtight container (see Fig. 2), which was sealed under the inert atmosphere of the evaporation chamber to avoid air exposure. The scanning measurements for cell 9 were performed in the same container after the current voltage curves were recorded.

## 3. Results

### 3.1. Efficiency patterns

The 10 investigated cells (Table 1) have yielded solar efficiencies of up to 2.6% (Fig. 3A). This cell yielded an initial short-circuit photocurrent density of 7.55 $mAcm^{-2}$ and a photovoltage of 0.754 V. The fill factor was determined to be 0.456. The effective solar cell area was 5.25 $mm^2$. It can be observed that this cell, analyzed with a laser spot of 10 μm diameter and an adjusted light intensity of 106 $W/m^2$ (much lower than solar light intensity) shows remarkable inhomogeneities. While about one-third of the cell surface yields a laser-induced photocurrent density of more than 80 $\mu A/cm^2$, the rest of the cell seems to operate at two-third of the maximum efficiency. Characteristic spots of 50–100 μm in diameter can be identified where the photocurrent efficiency reaches only 50% of that in the surrounding area. To rule out that the inhomogeneities are an effect of trivial morphological variations across the plastic solar cell, an image of reflected light (Fig. 3B) was also recorded. A more homogeneous reflection without the characteristic patterns is seen, as compared with the photocurrent image (Fig. 3A), ruling out trivial morphological variations across the plastic solar cell or related optical effects as an obvious reason for photocurrent inhomogeneities. They maybe induced to be controlled by impurities or impurity controlled reactivity of the composite.

Table 1
Experimental conditions and measurement program explained for different solar cells as presented in the listed figures

| Figure | Cell | Imageheight (mm) | Imagewidth (mm) | Light intens-ity ($W/m^2$) | Laser spot diameter (μm) | Pulse frequency (Hz) | Step size (μm) | Exposure to air | Dark storage |
|---|---|---|---|---|---|---|---|---|---|
| 3 a | 9 | 2.385 | 4.245 | 106 | 10 | 71 | 15 | Inert atm. | 1 day |
| 3 b | 9 | 2.250 | 3.870 | 106 | 10 | 109 | 30 | Inert atm. | 2 days |
| 4 | 9 | 2.480 | 4.360 | 1940 | 14 | 71 | 20 | 2 weeks | 2 weeks |
| 7 a | 1 | 2.820 | 7.380 | 835 | 18 | 69 | 20 | 1 h | 2 months |
| 7 b | 2 | 2.360 | 7.620 | 835 | 18 | 69 | 20 | 1 h | 2 months |
| 7 c | 2 | 2.550 | 7.290 | n.a. | 15 | 71 | 30 | 1 week | 2 months |
| 9 a | 10 | 2.160 | 4.800 | 2084 | 14 | 72 | 20 | 2 weeks | — |
| 9 b | 11 | 2.700 | 4.960 | 2011 | 14 | 78 | 20 | 2 weeks | — |
| 9 c | 12 | 2.420 | 5.160 | 2011 | 14 | 78 | 20 | 2 weeks | — |
| 11 a | 3 | 2.040 | 4.620 | 802 | 30 | 72 | 30 | 1 h | 3 months |
| 11 b | 4 | 1.980 | 5.900 | 800 | 30 | 71 | 20 | 1 h | 2 months |
| 11 c | 5 | 2.340 | 6.090 | 800 | 30 | 71 | 30 | 1 h | 2 months |
| 12 | 5 | 0.232 | 0.464 | n.a. | 2 | 73 | 2 | 1 day | 2 months |

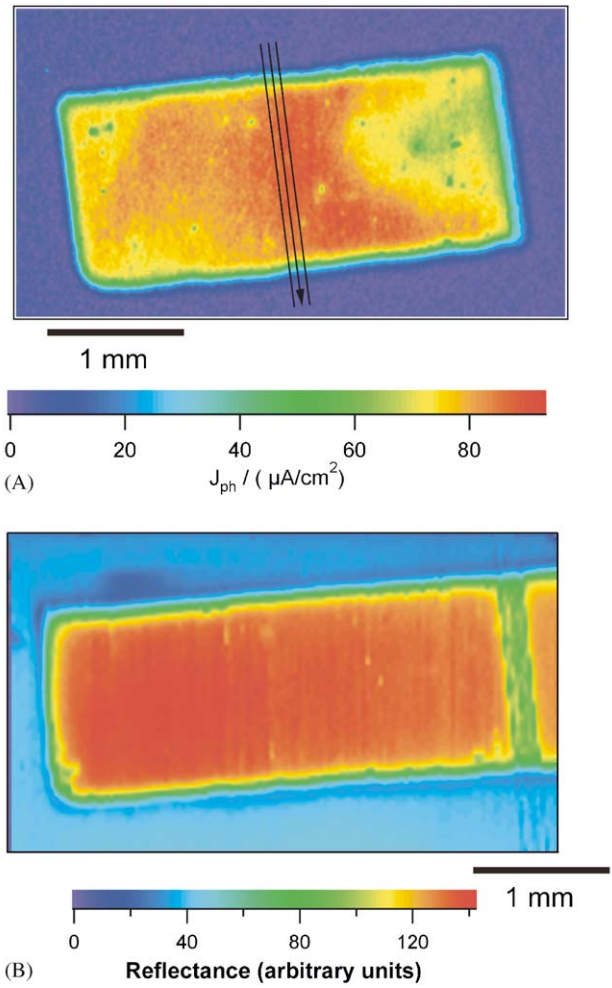


Fig. 3. Cell 9: Photocurrent density (A) and reflectance (B) diagram taken under air exclusion. The black arrow shows the position of the cross-section in Fig. 5. $J_{PH}$ = photocurrent density. The starting solar efficiency of the cell was 2.6%.

Fig. 4 shows the same cell as in Fig. 3, after dark degradation in air for 2 weeks. The obtained photocurrent pattern differs from the original cell. It looks blurred, an effect of the high light intensity (1940 W/m$^2$) used to obtain the image of the much degraded photocurrent. A curious feature in Fig. 4 is an isolated area with somewhat higher photocurrent density. The boundaries of the cell yield lower photocurrent than the bulk, which looks less decomposed. This can be seen more clearly in the photocurrent profiles across the plastic cells, presented in Fig. 5 for the fresh cell (Fig. 3) and the decomposed cell (Fig. 4). A lateral process of degradation of the

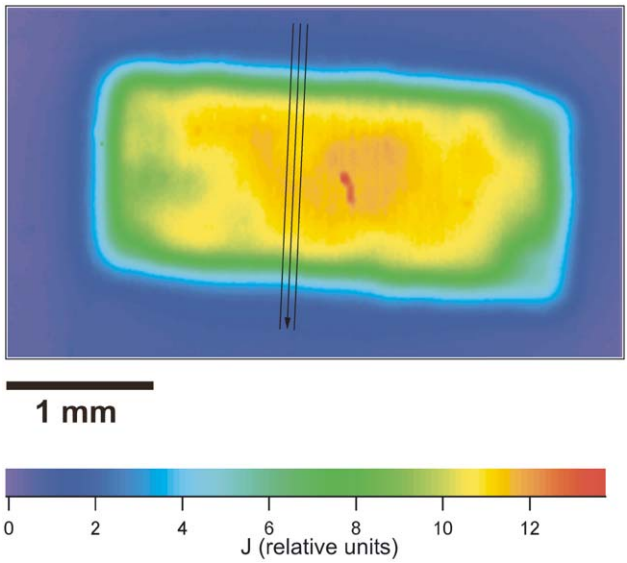


Fig. 4. Cell 9: Photocurrent density image after degradation in air in the dark for 2 weeks. Some degree of deterioration at the edges can be observed. The black arrow shows the position of the cross-section in Fig. 5.

solar cell may be taking place simultaneously to degradation through diffusion of ambient gases into the aluminum cover layer. The photocurrent voltage characteristics of the plastic cell from Fig. 3 are shown in a linear and a logarithmic current plot (Fig. 6). This curve was taken in an inert atmosphere before recording the images.

### 3.2. *Inhomogeneous aluminum deposits*

A few of the plastic solar cells, with efficiencies of 1.0–1.5%, showed significant inhomogeneities due to a preparation step. In the case of Fig. 7a and b, aluminum contact deposition created an evaporation shadow pattern with a significantly enhanced photocurrent. On the right rim of the plastic cell in Fig. 7a, the photocurrent density turned out to be three times as high as in the rest of the plastic cell area. This is a remarkable observation indicating that the Al deposition conditions are crucial to achieving high efficiencies. To find out more about the cause of the patterns an image of reflectance was measured (Fig. 7c) where the patterns were not observed, ruling out optical effects. To dermine whether variations in aluminum thickness correlate with the observed photocurrent, DEKTAK profile measurements were performed along the arrows a, b, c in Fig. 7. Fig. 8 shows the profiles. Surprisingly no change of thickness is observed within the area of high photocurrent density. Since the pattern of aluminum shadowing was measured with

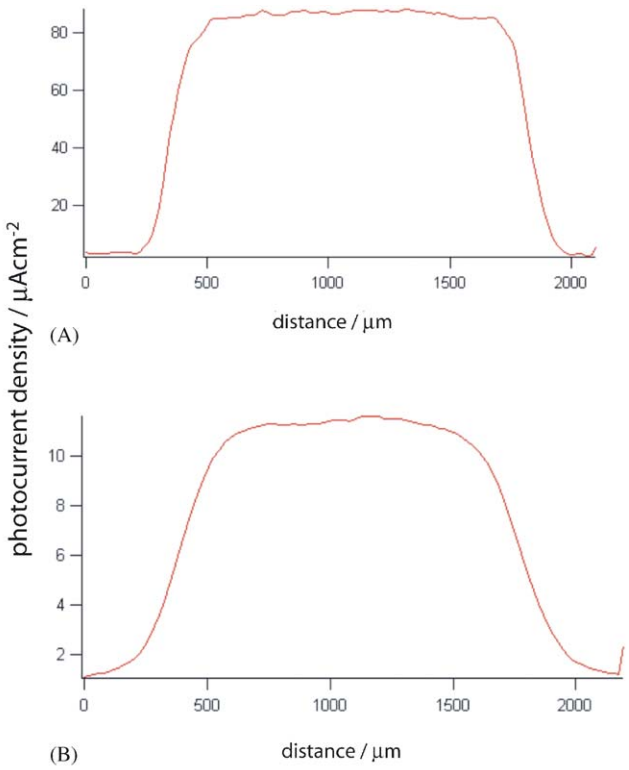


Fig. 5. Cross-section of photocurrent density through cell 9 in an inert atmosphere (A) and after 2 weeks of degradation in air (B).

a laser spot dimension of 18 µm the information obtained appears to be reliable. The nature of Al/polymer composite interface seems to play a key role in the efficiency of electron and hole transfer. However, more systematic measurements will be necessary to clarify possible mechanisms.

### 3.3. *Patterns of degradation*

Fig. 9 shows the degradation of the photocurrent of a plastic solar cell under 1000 W/cm$^2$ illumination inside the sealed container, used for cell 9. Already within 1 h the effect is very pronounced. It also shows how a temporary exposure of the cell to air leads to an accelerated decrease of photoefficiency, and gives a measure of the cells lifetime for the measurements used for cell 9. Fig. 10 shows three cells after 2 weeks of degradation. The photocurrent seems to become inhomogeneous, suggesting selective degradation. Higher degrees of degradation around the rim of the cell could be an effect of a mechanism of lateral degradion through diffusion of oxygen or water vapor.

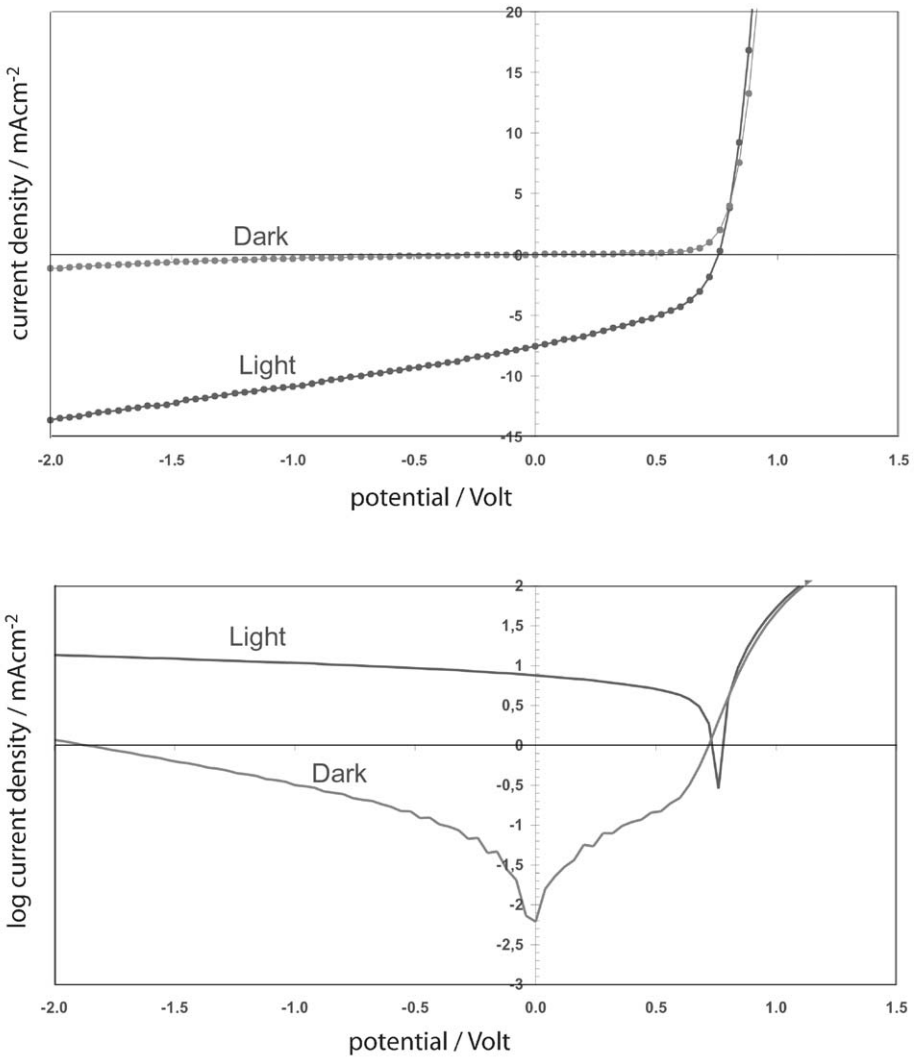


Fig. 6. Current–voltage characteristics of cell 9 in the dark and under 1000 W/m$^2$ illumination, taken prior to scanning photocurrent microscopy under an inert atmosphere.

### 3.4. Island formation

Fig. 11 shows photocurrent images of three plastic solar cells after 2 months of dark storage. The cells have characteristically altered the pattern of photocurrent efficiency distribution. They exhibit island-like areas with still enhanced photocurrent efficiency. Some areas of composite aggregation seem to be more stable than others. To determine whether the decomposed areas exhibit a

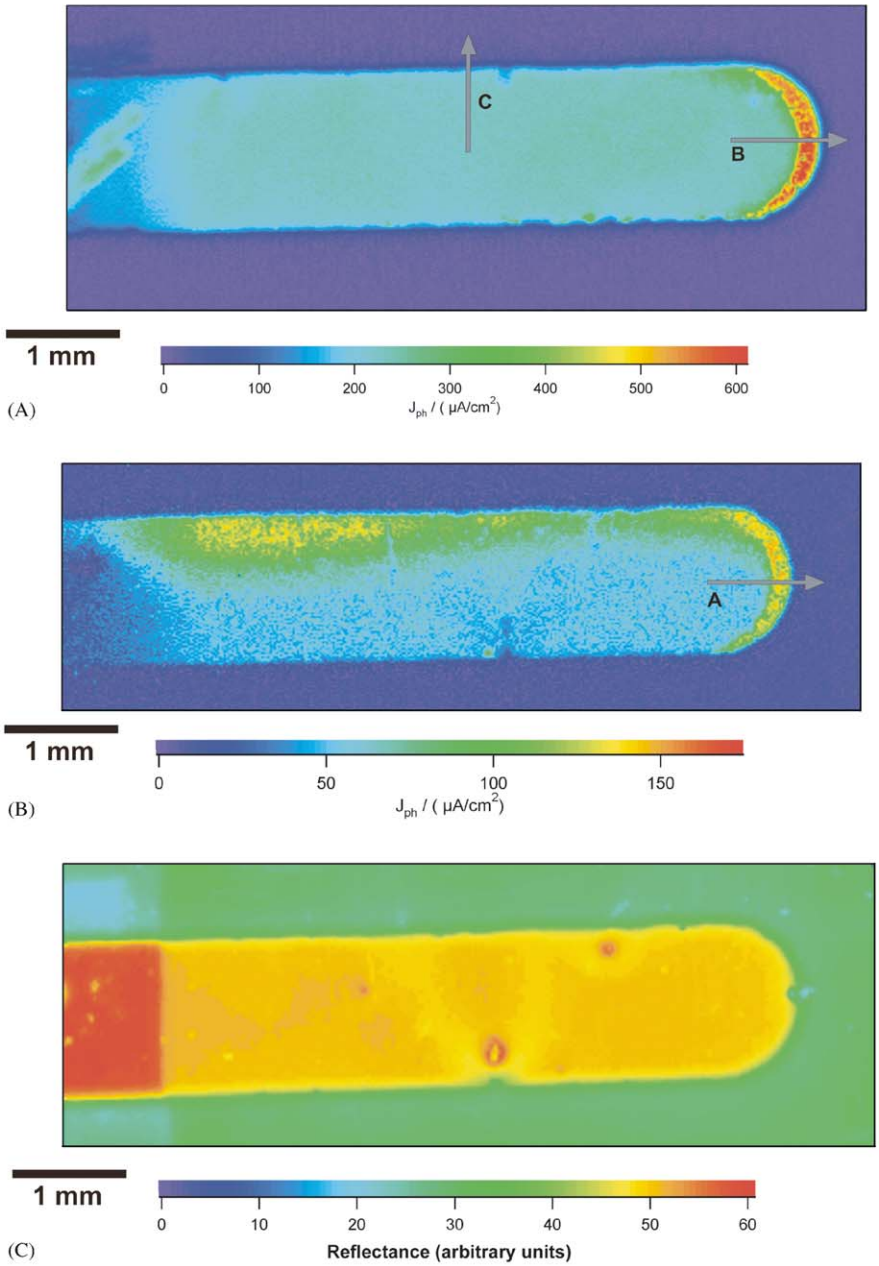


Fig. 7. Photocurrent density patterns caused by a shadow during aluminum vacuum deposition. Photocurrent density is larger in the shadow region in cell 1 (A) and cell 2 (B). A reflectance image of cells 2 (C) shows that the shadow is probably not an optical effect. The arrows on cells 1 and 2 indicate the locations of DEKTAK measurements.

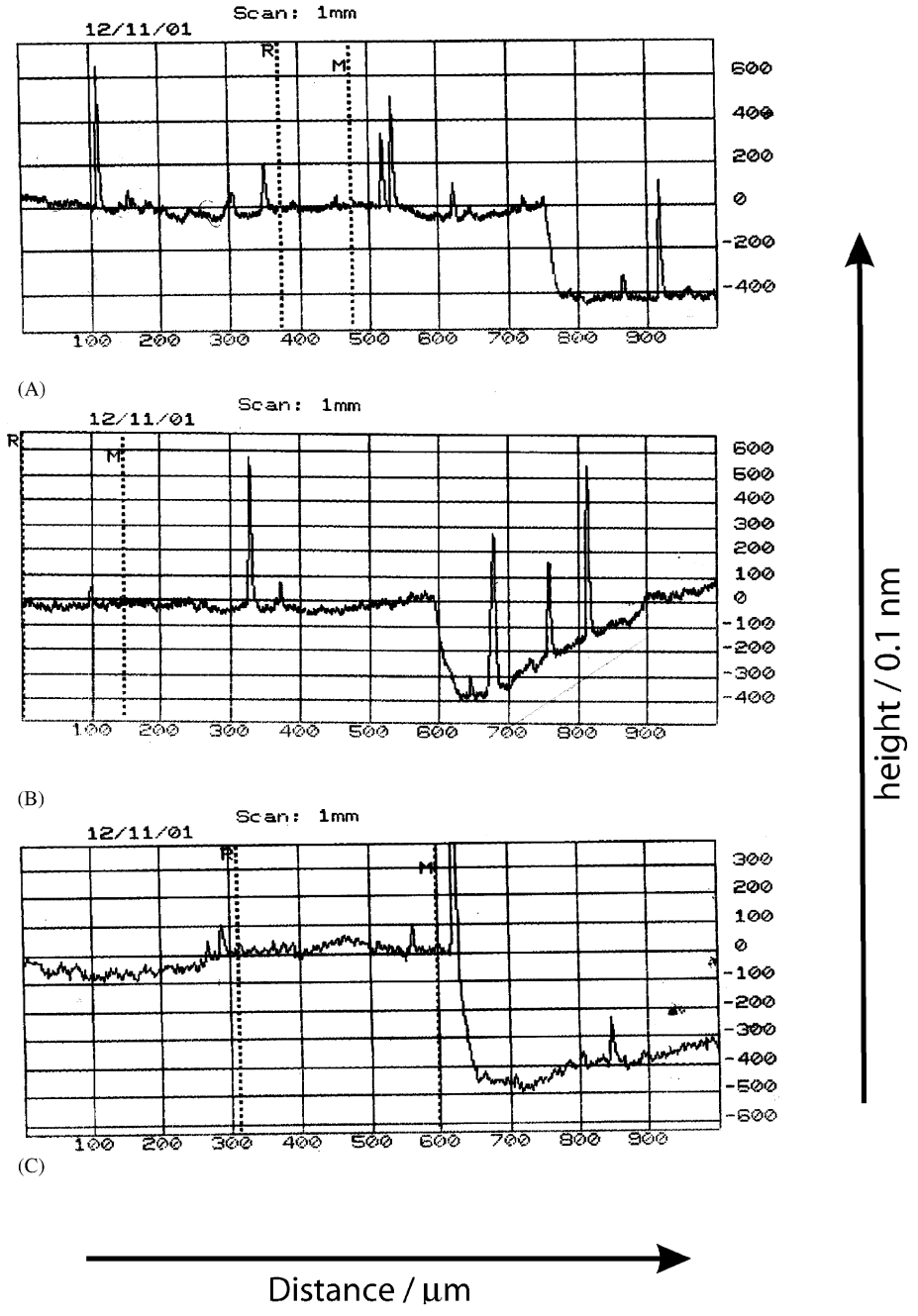


Fig. 8. DEKTAK profiles of cells 1 and 2, taken at the edge of the aluminum strip. Graphs A, B, C correspond to arrows on Fig. 7. Units are in mm on the $x$-axis and Angstroms on the $y$-axis. A step of about 400 Å (40 nm), seen in all three profiles, is probably the edge of the aluminum strip. No change in thickness due to the shadow can be observed at the expected position 200 µm before the edge in (A) and (B).

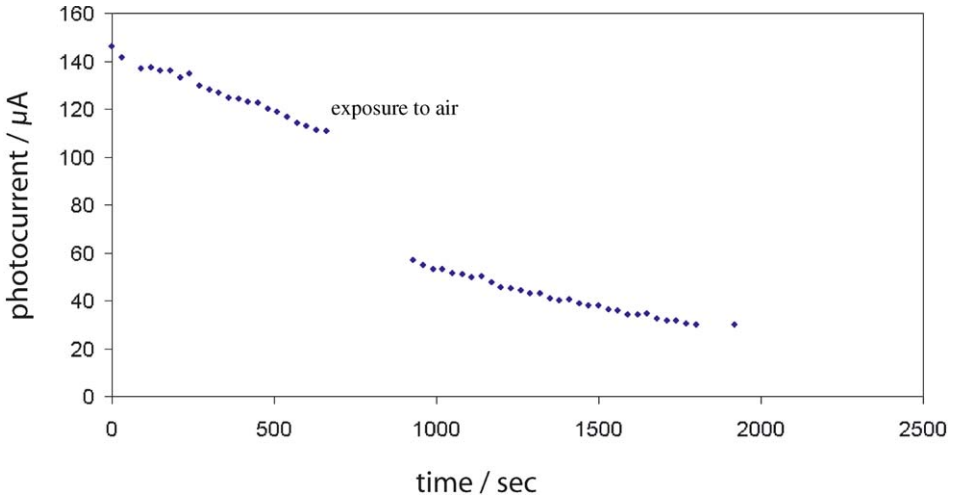


Fig. 9. Decay of photocurrent ($I_{sc}$) in Cell 10 as a result of degradation under 1000 W/cm$^2$ illumination in an inert atmosphere, followed by exposure to the atmosphere.

micrometer-scale structure, photocurrent images with a laser spot of 2 μm diameter were performed (Fig. 12) and a smooth pattern was observed, indicating an absence of efficiency determining crystalline or polymeric structures on this scale.

## 4. Discussion

This explorative study of photocurrent images of plastic solar cells has yielded some interesting results, which warrant further detailed investigation. First it was observed that the photocurrent density of plastic solar cells is usually inhomogeneous to some extent, indicating that a significantly higher efficiency is within reach, for example by more accurate control of the process of plastic cell fabrication. The remarkable threefold increase of photocurrent density as a result of beam shadows during aluminum deposition is apparently a phenomenon, which has been caused by the geometry of chamber and masks influencing the local nature of the deposition process. It indicates that there are challenging problems related to forming metal contacts with polymer: fullerene solar cells. A weakness of plastic solar cells is their instability, both in presence of light and in the dark as well as upon exposure to ambient gases such as oxygen and water vapor. The apparently characteristic property of these plastic solar cells of allowing islands of high efficiency to survive suggests that there is room for more understanding and improvement. The presented experiments have shown that photocurrent images yield additional information to integral measurements. Peculiarities and random variations of parameters, of which there are a great number in this type of device, can be tracked down faster with this

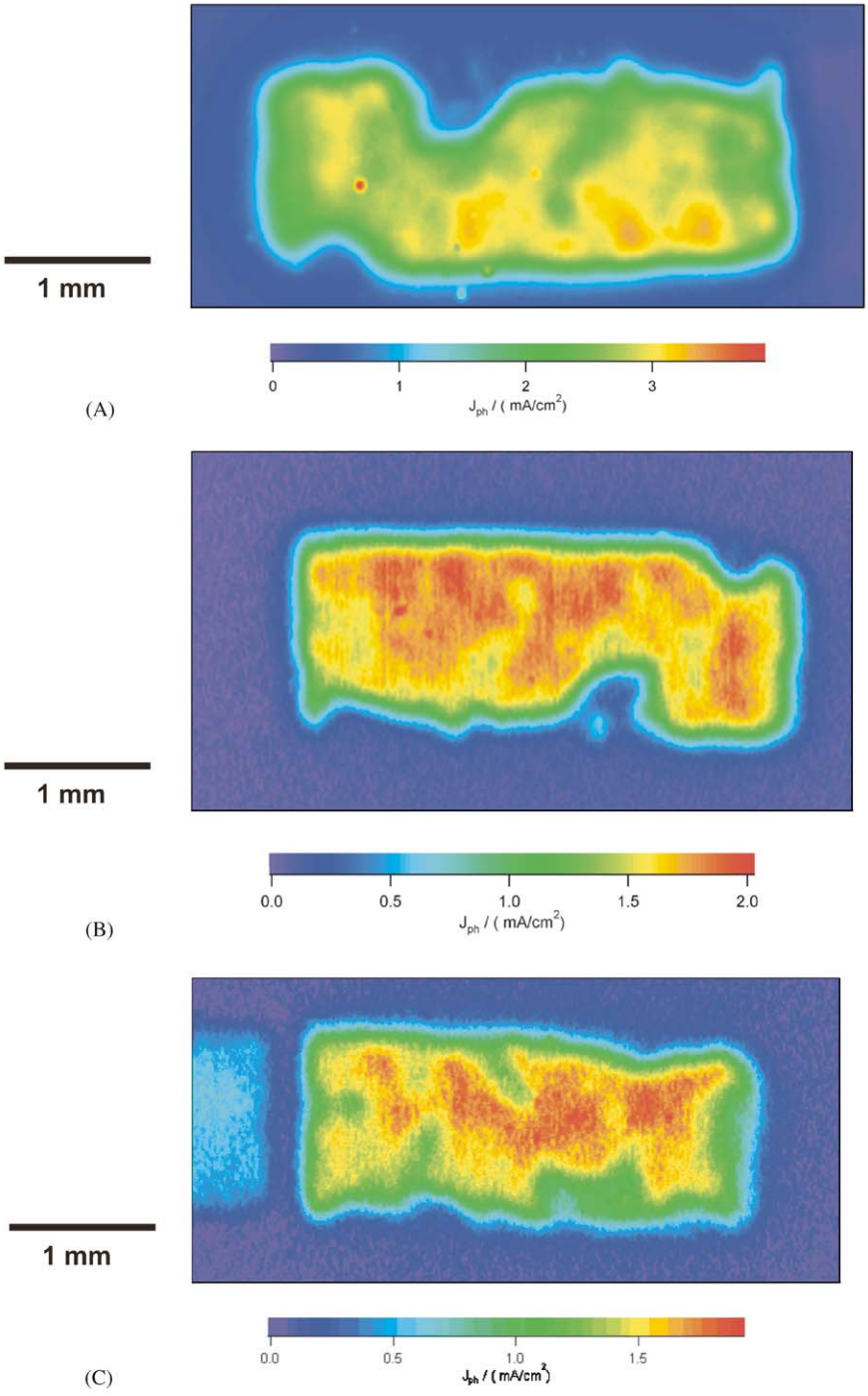


Fig. 10. Photocurrent density images of cells 10, 11 and 12 (A, B and C, respectively) after 2 weeks degradation.

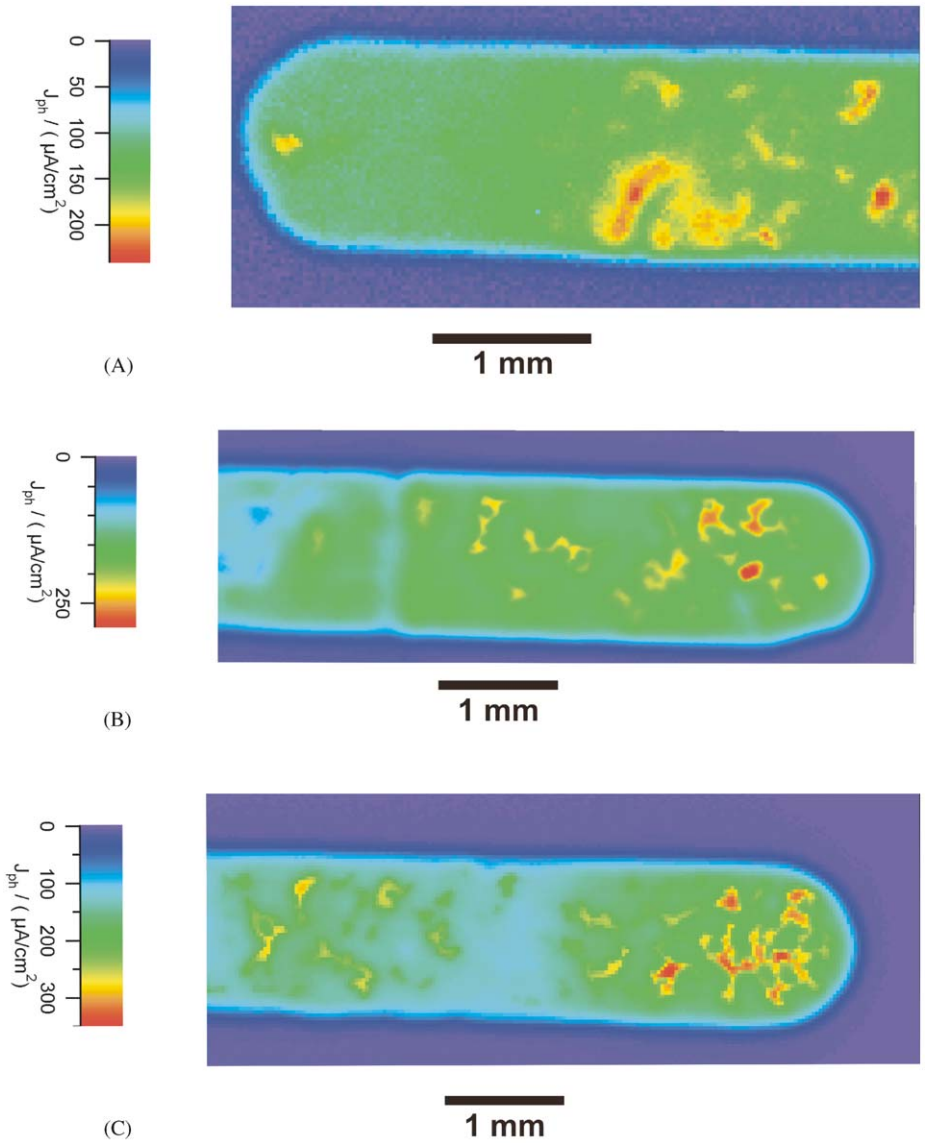


Fig. 11. Photocurrent density images of cells 3, 4 and 5 (A, B and C, respectively) after 2 months of dark storage.

method. The technique also has potential in combinatorial research of plastic solar cells. It allows local modificaton of a cell with chemical or physical factors and observation of the induced changes during an aging process, avoiding the inevitable

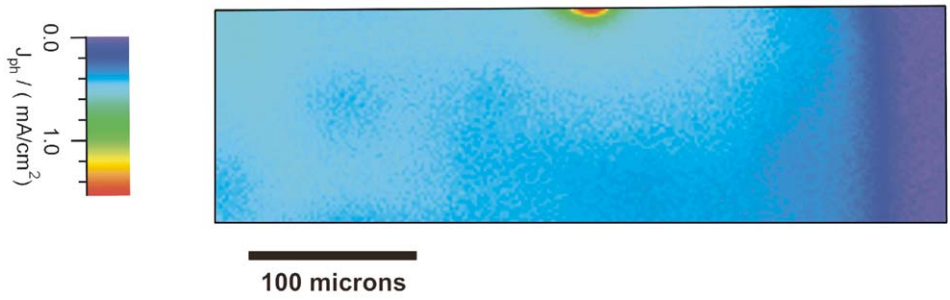


Fig. 12. High-resolution photocurrent density image of cell 5. The homogeneous pattern suggests that no fine structure (e. g. due to fibers or aggregates) exists at 2 μm resolution.

quality variations between different samples in traditional experiments. It may be possible to obtain a more rapid cell optimization in this way.

## Acknowledgements

The authors would like to thank Mr. A. Barkschat for introduction and access to his photocurrent imaging setup and Prof. Weidinger's group at the HMI for constructive experimental cooperation.

## References

[1] G. Yu, J. Gao, J.C. Hummelen, F. Wudl, A.J. Heeger, Science 270 (1995) 1789.
[2] N.S. Sariciftci, A.J. Heeger, in: H.S. Nalwa (Ed.), Handbook of Organic Conductive Molecules and Polymers, Vol. 1, Wiley, New York, 1997.
[3] C.J. Brabec, N.S. Sariciftci, J.C. Hummelen, Adv. Funct. Mater. 11 (2001) 15; C.J. Brabec, N.S. Sariciftci, in: G. Hadziannou, P. van Hutten (Eds.), Conjugated Polymers, Wiley-VCH, Weiningen, 1999.
[4] G.S.E. Shaheen, C.J. Brabec, F. Padinger, T. Fromherz, J.C. Hummelen, N.S. Sariciftci, Appl. Phys. Lett. 78 (1995) 841.
[5] C.J. Brabec, G.S.E. Shaheen, T. Fromherz, F. Padinger, J.C. Hummelen, A. Dhanabalan, R.A.J. Janssen, N.S. Sariciftci, Synth. Met. 121 (2001) 1517.
[6] C.J. Brabec, A. Cravino, D. Meissner, N.S. Sariciftci, T. Fromherz, M.T. Rispens, L. Sanchez, J.C. Hummelen, Adv. Fund. Mater. 11 (2001) 374.
[7] M. Turrión, B. Macht, P. Salvador, H. Tributsch, Z. Phys. Chem. 212 (1999) 51–57.
[8] B. Macht, M. Turrión, A. Barkschat, P. Salvador, K. Ellmer, H. Tributsch, Sol. Energy Mater. Sol. Cells 73 (2002) 163–173.